PIP30/FAM192A is a novel regulator of the nuclear proteasome activator PA28γ

Beata Jonik-Nowak[a,1], Thomas Menneteau[b,1], Didier Fesquet[a,1], Véronique Baldin[a], Catherine Bonne-Andrea[a], Francisca Méchali[a], Bertrand Fabre[b], Prisca Boisguerin[a], Sylvain de Rossi[c], Corinne Henriquet[d], Martine Pugnière[d], Manuelle Ducoux-Petit[b], Odile Burlet-Schiltz[b], Angus I. Lamond[e], Philippe Fort[a], Séverine Boulon[a,2], Marie-Pierre Bousquet[b,2], and Olivier Coux[a,2]

[a]Centre de Recherche en Biologie Cellulaire de Montpellier (CRBM), Université de Montpellier, CNRS, 34090 Montpellier, France; [b]Institut de Pharmacologie et Biologie Structurale (IPBS), CNRS, Université de Toulouse–Université Paul Sabatier, 31062 Toulouse, France; [c]Montpellier Ressources Imagerie (MRI) Facility, Biocampus UMS3426, CNRS, 34090 Montpellier, France; [d]Institut de Recherche en Cancérologie de Montpellier (IRCM) - INSERM U1194, Institut Régional du Cancer de Montpellier, Université de Montpellier, F-34298 Montpellier, France; and [e]Centre for Gene Regulation and Expression, School of Life Sciences, DD1 5HL Dundee, United Kingdom

Edited by Alfred Lewis Goldberg, Harvard Medical School, Boston, MA, and approved May 29, 2018 (received for review December 21, 2017)

PA28γ is a nuclear activator of the 20S proteasome involved in the regulation of several essential cellular processes, such as cell proliferation, apoptosis, nuclear dynamics, and cellular stress response. Unlike the 19S regulator of the proteasome, which specifically recognizes ubiquitylated proteins, PA28γ promotes the degradation of several substrates by the proteasome in an ATP- and ubiquitin-independent manner. However, its exact mechanisms of action are unclear and likely involve additional partners that remain to be identified. Here we report the identification of a cofactor of PA28γ, PIP30/FAM192A. PIP30 binds directly and specifically via its C-terminal end and in an interaction stabilized by casein kinase 2 phosphorylation to both free and 20S proteasome-associated PA28γ. Its recruitment to proteasome-containing complexes depends on PA28γ and its expression increases the association of PA28γ with the 20S proteasome in cells. Further dissection of its possible roles shows that PIP30 alters PA28γ-dependent activation of peptide degradation by the 20S proteasome in vitro and negatively controls in cells the presence of PA28γ in Cajal bodies by inhibition of its association with the key Cajal body component coilin. Taken together, our data show that PIP30 deeply affects PA28γ interactions with cellular proteins, including the 20S proteasome, demonstrating that it is an important regulator of PA28γ in cells and thus a new player in the control of the multiple functions of the proteasome within the nucleus.

proteasome | PA28γ | Cajal bodies | FAM192A | nuclear proteolysis

The 20S proteasome is a multimeric "barrel-like" protease that bears multiple peptidase (i.e., trypsin-like, caspase-like, and chymotrypsin-like) activities inside its internal catalytic chamber (1). It plays a major role in the regulated degradation of intracellular proteins and requires for its functioning, in most cases, the binding of regulatory complexes to one or both of its ends (1). Among these regulators, the well-characterized 19S regulatory complex has been shown to associate with the 20S core to form the 26S proteasome that specifically recognizes and degrades polyubiquitylated proteins (2, 3). Another type of 20S proteasome regulators is the PA28 (also called 11S or REG) family of complexes, which comprises in higher eukaryotes three related proteins (PA28α, -β, and -γ) that associate in two distinct complexes (4). PA28α and PA28β form a cytoplasmic heteroheptamer, PA28αβ (5, 6), which participates in the immune response by favoring the generation of MHC class I antigens (7, 8). In contrast, PA28γ is essentially nuclear and forms a homoheptamer (9, 10). PA28 complexes mediate primarily ubiquitin-independent proteolysis when bound to the 20S proteasome. However, they are also found in hybrid proteasomes (i.e., 20S proteasome bound to a PA28 heptamer on one end and a 19S complex on the other end) (11) and are thus likely to also participate in ATP-dependent degradation of ubiquitylated proteins.

Although PA28γ has been little studied, it is involved in various essential cellular pathways, including cell proliferation, through the degradation of the cell cycle inhibitors $p21^{Cip1}$, $p16^{INK4A}$, and $p19^{Arf}$ (12–14). PA28γ also participates in the Mdm2-dependent degradation of the tumor suppressor p53 (15). Furthermore, $PA28\gamma^{-/-}$ mice display growth retardation (16) and PA28γ is overexpressed in several types of cancer (17–19). In addition to its involvement in the control of cell proliferation, PA28γ is implicated in the regulation of chromosomal stability (20) and plays important roles in nuclear dynamics by modulating the number and size of various nuclear bodies, including Cajal bodies (CBs) (21), nuclear speckles (22), and promyelocytic leukemia protein bodies (23). It is also involved in the cellular stress response, as it is recruited to double-strand break sites upon DNA damage (24) and is required for the UVC-induced dispersion of CBs (21).

Despite its important cellular functions, the mechanisms of action of PA28γ, like those of the related PA28αβ complex, remain elusive. It is known that, like the 19S complex, PA28 complexes open the gated pore of the 20S proteasome's α-ring upon binding, thus allowing easier substrate entrance into the catalytic chamber (25). Artificial peptide substrates commonly used to measure proteasome activities are believed to passively

Significance

The 20S proteasome is a key actor of the control of protein levels and integrity in cells. To perform its multiple functions, it works with a series of regulators, among which is a nuclear complex called PA28γ. In particular, PA28γ participates in the regulation of cell proliferation and nuclear dynamics. We describe here the characterization of a protein, PIP30/FAM192A, which binds tightly to PA28γ and favors its interaction with the 20S proteasome while inhibiting its association with coilin, a central component of nuclear Cajal bodies. Thus, PIP30/FAM192A critically controls the interactome and, consequently, the functions of PA28γ, and appears to be a previously unidentified player in the fine regulation of intracellular proteostasis in the cell nucleus.

Author contributions: O.B.-S., A.I.L., S.B., M.-P.B., and O.C. designed research; B.J.-N., T.M., D.F., V.B., C.B.-A., F.M., B.F., P.B., C.H., M.P., M.D.-P., P.F., S.B., M.-P.B., and O.C. performed research; S.d.R. contributed new reagents/analytic tools; B.J.-N., T.M., D.F., V.B., C.B.-A., F.M., B.F., P.B., C.H., M.P., M.D.-P., O.B.-S., A.I.L., P.F., S.B., M.-P.B., and O.C. analyzed data; and P.F., S.B., M.-P.B., and O.C. wrote the paper.

The authors declare no conflict of interest.

This article is a PNAS Direct Submission.

[1]B.J.-N., T.M., and D.F. contributed equally to this work.

[2]To whom correspondence may be addressed. Email: severine.boulon@crbm.cnrs.fr, Marie-Pierre.Bousquet@ipbs.fr, or olivier.coux@crbm.cnrs.fr.

This article contains supporting information online at www.pnas.org/lookup/suppl/doi:10.1073/pnas.1722299115/-/DCSupplemental.

Published online June 22, 2018.

CELL BIOLOGY

diffuse through the 20S pores, and therefore PA28s' stimulation of their degradation can be explained by 20S-pore opening only. However, how PA28 complexes recruit protein substrates and deliver them to the proteasome is not understood, as these complexes are a priori inert molecules that, unlike the 19S complex, do not possess any ATPase activity that could provide energy and movement to unfold the substrates and inject them into the 20S proteasome (2, 3). A likely possibility is thus that PA28 complexes function in proteasome-dependent proteolysis in association with other proteins that remain to be defined.

In this study, we describe a partner of a PA28 complex, the evolutionary conserved PIP30/FAM192A protein. We show that PIP30 binds with high specificity to PA28γ and enhances its association with the 20S proteasome in cells. Importantly , PIP30 binding affects PA28γ specificity toward peptide substrates in vitro as well as its interactions with cellular proteins, such as the CB marker coilin. Therefore, PIP30 is a major regulator of PA28γ functions and consequently of the nuclear functions of the proteasome.

Experimental Procedures

Phylogenetic Analyses. Genomes were explored by using Annotation and BLAST search tools available in the Geneious 9.1.7 software package (www.geneious.com/). Amino acid sequences were aligned (MAFFT v7.017) and a phylogenetic tree was deduced by maximum-likelihood analysis (PhyML).

Antibodies. Antibodies and related agents used in this study are described in *SI Appendix, Material and Methods*.

Production of 20S Proteasome and Recombinant Proteins. Native 20S proteasome was purified from extracts of HeLa cells (Ipracell) using classic chromatographic procedures (26). Unless indicated, recombinant PIP30 was produced in *Escherichia coli* BL21 DE3 CodonPlus as a 6His-tagged protein and purified by affinity purification followed by proteolytic removal of the tag, anion-exchange chromatography, and gel filtration (*SI Appendix*, Fig. S10*B*). At the last step, the protein was eluted slightly earlier than the BSA (67 kDa) marker (i.e., at an apparent molecular weight larger than twice what was expected). Human recombinant PA28αβ was produced and purified from *E. coli*, as previously described (27). Human PA28γ was expressed in *E. coli* BL21 DE3 CodonPlus. After expression, the PA28γ complex was purified by chromatography as PA28αβ, with some minor modifications of the procedure. Both PA28αβ and PA28γ complexes efficiently activated the peptidase activities of the 20S proteasome. Recombinant GST and GST-PIP30-H201 fusion proteins were produced in bacteria and efficiently purified using glutathione Sepharose beads.

Pull-Down and Immunoprecipitation. For immunoprecipitation (IP) of GFP-fusion proteins, U2OS cells were transfected with the indicated constructs. Twenty-four hours posttransfection, cells were homogenized in lysis buffer [25 mM Hepes pH 7.8, 100 mM KCl, 10 mM $MgCl_2$, 1 mM EDTA, 1% IGEPAL CA-630, 0.1% Triton X-100, 1 mM DTT, 1 mM ATP, 10% glycerol (vol/vol)], in the presence of complete EDTA-free protease inhibitor mixture (Roche), for 15 min on ice. After centrifugation at 15,000 × *g* for 15 min (4 °C), supernatants were recovered and protein concentration was determined by Bradford assays using BSA as a standard. Next, 20 μL of GFP-TRAP-A beads (Chromotek) were used per IP, mixed with 200 μg of protein extract, and incubated with constant gentle stirring for 1 h at 4 °C. Beads were washed three times with lysis buffer and boiled in 2× Laemmli sample buffer. Samples were then analyzed by SDS/PAGE and immunoblotting.

Endogenous PIP30 and PA28γ were immunoprecipitated from total cell extracts using anti-PIP30 (rabbit) and anti-PA28γ (rabbit) antibodies, bound to protein A magnetic beads (Dynal) for 2 h at 4 °C.

For co-IP of coilin and PA28γ proteins (see, for example, Fig. 5*B*), nuclear extracts were prepared as described in ref. 21. Briefly, U2OS and PIP30$^{-/-}$ cell pellets were resuspended in hypotonic buffer (10 mM Tris·HCl pH 7.5, 10% glycerol, 4 mM DTT, 50 mM NaF, 1 mM Na_3VO_4, 1 mM $MgCl_2$) in the presence of complete EDTA-free protease inhibitor mixture (Roche). IGEPAL CA-630 was then added at the final concentration of 0.5% and cells were incubated on ice for 3 min. After centrifugation at 800 × *g* for 5 min, the nuclei, present in the pellet, were resuspended in digestion buffer (2 mM Tris·HCl pH 8.5, 20% glycerol, 10 mM DTT, 50 mM NaF, 1 mM Na_3VO_4, 1 mM $MgCl_2$, 5 mM $CaCl_2$, 1× complete protease inhibitor mixture) supplemented with 75 U/mL micrococcal nuclease, and then digested for 15 min at 25 °C with constant stirring. At the end, an equivalent volume of extraction buffer (2 mM Tris·HCl pH 8.5, 50 mM NaF, 1 mM Na_3VO_4, 1 mM $MgCl_2$, 20 mM EDTA, 0.84 M KCl, 1× complete protease inhibitor mixture) was added and the mix was incubated on ice for 20 min. Nuclear extracts were clarified by centrifugation for 30 min at 15,000 × *g*. Before IP, KCl concentration was reduced to 280 mM, 3 μg of anticoilin or control IgG were added to 400 μg of nuclear extracts and incubated for 2 h at 4 °C. IP proteins were collected by addition of 15 μL of protein A-Sepharose beads. After extensive washes, beads were boiled in 2× Laemmli sample buffer and samples were analyzed by SDS/PAGE and immunoblotting.

Mass Spectrometry Analyses. Stable isotope labeling by amino acids in cell culture (SILAC) IPs (endogenous PA28γ and GFP-FAM192A/PIP30) were essentially performed as previously described in ref. 28. Further details are provided in *SI Appendix*.

Whole human proteasome complexes, including 20S-bound activators and regulators, were immunopurified and analyzed by quantitative mass spectrometry, as previously described (29, 30). Next, 2×10^8 in vivo formaldehyde–cross-linked human cells (HeLa and U937, three biological replicates per cell line) were used. For complete nuclear proteasome interactome analysis, U937 cells nuclei were prepared and, before proteasome purification, the purity of nuclear proteins was assessed both by Western blot and MS analysis, as detailed earlier (31). Purified proteasome complexes were analyzed by mass spectrometry as previously described (32). Further details are provided in *SI Appendix* section.

Native Electrophoresis in Tris-Glycine System. Recombinant protein samples were incubated 5–10 min at room temperature in reaction buffer [Tris·HCl 20 mM, pH 7.5, DTT 1 mM, Glycerol 10% (vol/vol)], then supplemented with 1 μL of native sample buffer (xylene cyanol FF in reaction buffer supplemented with 50% glycerol) and applied on 5% polyacrylamide gel prepared in Tris-Glycine electrophoresis buffer (25 mM Tris·HCl pH 8.0, 192 mM Glycine, 1 mM DTT). Native electrophoresis was performed for 4–5 h (100 V, 4 °C). After denaturation in 10× TG-SDS buffer, proteins were transferred on PVDF membrane and immunoblotted.

Surface Plasmon Resonance Analysis. Experiments were performed on Biacore 3000 apparatus (GE Healthcare) at 25 °C using a flow rate of 50 μL/min in HBS-EP buffer (GE Healthcare). To compare the binding of PA28γ and PA28αβ on 6His-PIP30 recombinant protein, 6His-PIP30 (4500RU) was captured on anti–His-Tag covalently immobilized on a CM5 sensor chip using an amine coupling procedure according to the manufacturer's instructions. A control flowcell was obtained with the same chemical procedure without protein. Then, 60 μL of PA28γ and PA28αβ (50 μg/mL) were injected on His6PIP30 and control flowcells followed by a dissociation step of 400 s.

In Vitro CK2 Phosphorylation Assay. GST and GST-PIP30-H201 proteins were incubated with recombinant CK2 according to the manufacturer's instructions. For radioactive kinase assays, ^{33}P labeled ATP (1 μCi in the presence of 100 μM cold ATP) was included. Reactions were stopped either by adding 5 mM EDTA or Laemmli sample buffer.

Proteasome Peptidase Assays. Peptidase activities of 20S proteasome were measured using black flat-bottom 96-well plates (Nunc), in a final volume of 50 μL, in reaction buffer [20 mM Tris·HCl pH 7.5, 50 mM NaCl, 1 mM DTT, 10% glycerol (vol/vol)] supplemented with 100 μM peptide substrates. When indicated, purified recombinant PA28 and/or PIP30 were added. Kinetic analyses showed that the assays are linear at least for 30 min. Peptide degradation was measured by the fluorescence emitted by the AMC group released by cleavage of the substrate (excitation 380 nm, emission 440 nm) using a FLx800 microplate fluorescence reader (Bio-Tek Instruments).

Immunofluorescence Microscopy and Proximity Ligation Assays. Cells were fixed in 3.7% paraformaldehyde/PBS for 10 min at room temperature, washed with PBS and permeabilized in PBS containing 1% Triton X-100 for 15 min at room temperature. Coverslips were then blocked in blocking solution (1% FCS, 0.01% Tween-20/PBS) for 10–20 min and incubated with primary antibodies, diluted in blocking buffer, for 1 h at room temperature or 37 °C in a humidified atmosphere. After three washes in PBS, coverslips were incubated with Alexa-Fluor conjugated secondary antibodies diluted in blocking solution for 40 min at room temperature. Coverslips were washed with PBS, incubated with 0.1 μg/mL DAPI solution in PBS for 5 min at room temperature, washed twice in PBS, and finally once in H_2O. Coverslips were mounted on glass slides using ProLong Gold antifade reagent (Thermo Fisher Scientific).

For proximity ligation assays (PLA), cells on coverslips were fixed and permeabilized as described in ref. 22. Coverslips were then blocked in a

solution provided by the Duolink kit. Cells were then incubated with mentioned antibodies as described above. Duolink In Situ PLA Probe Anti-Rabbit MINUS and Anti-Mouse PLUS and Duolink In Situ Detection Reagents (Sigma-Aldrich) were used, according to the manufacturer's instructions.

Image Acquisition and Analysis. The *z*-stacks and images were acquired with a 63×/1.4 NA or 40× oil-immersion objective lenses using widefield microscopes, DM6000 (Leica Microsystems) or Axioimager Z1 or Z2 (Carl Zeiss), equipped with coolSNAP HQ2 cameras (Photometrics). Images were acquired as TIF files using MetaMorph imaging software (Molecular Devices). For CB and PLA dot quantitative analysis, *z*-stacks were acquired every 0.3–0.4 μm (*z*-step) with a range of 10–15 μm to image the whole nuclei. The number of PLA foci was analyzed with ImageJ. The size, the intensity, and the number of CBs were measured with ImageJ (1.49v), using a specific "macro" that has been created to automatically quantify these different parameters. The script allows creating a mask of DAPI image to isolate the nucleus of each cell and create a maximum-intensity projection of the 25 *z*-stacks. The mask is used in the maximum-intensity projection to count the number of CB or PLA dots of each nucleus via an appropriate thresholding. The "Analyze Particles" tool of ImageJ was used to calculate the size and the mean gray value of each CB.

Results

FAM192A Is a Partner of both Free and 20S Proteasome-Bound PA28γ That Regulates the Interaction Between PA28γ and 20S Proteasome. To identify new interactors of PA28γ, we used a high-throughput approach combining endogenous PA28γ IP and SILAC-based quantitative proteomics (28) (*SI Appendix*, Fig. S1*A*, *Left*). In this experiment, 68 human protein groups containing at least two unique peptides were quantified and visualized by plotting $\log_2$[heavy/light (H/L) ratio] versus $\log_2$(H intensity) (Fig. 1*A* and Dataset S1). PA28γ itself was found with a H/L SILAC ratio close to 15. Among the PA28γ interactors was FAM192A, a poorly annotated nuclear protein of unknown cellular function, whose expression is induced during skeletal muscle atrophy (33). FAM192A was also identified with a high SILAC ratio in a GFP-PA28γ pull-down that we performed in parallel (Dataset S2). Conversely, PA28γ was the most abundant and almost unique partner pulled down with GFP-FAM192A (Fig. 1*B* and *SI Appendix*, Fig. S1*A*, *Right* and Dataset S3). Reciprocal IPs on endogenous proteins showed that at least 70% of each protein coprecipitates with the other (*SI Appendix*, Fig. S1*B*). Like PA28γ, FAM192A is nuclear (*SI Appendix*, Fig. S10*A*) and interaction between the two proteins occurs within the nucleus (*SI Appendix*, Fig. S1*C*).

Using recombinant FAM192A and PA28γ proteins produced in *E. coli*, we found that the interaction between FAM192A and PA28γ is direct, as shown for example by native gel electrophoresis (Fig. 1*C*) or surface plasmon resonance (SPR) (*SI Appendix*, Fig. S1*D*). SPR showed no interaction between FAM192A and the closely related PA28αβ complex (*SI Appendix*, Fig. S1*D*), demonstrating the high specificity of PA28γ/FAM192A interaction in vitro.

Through parallel approaches, we investigated putative nuclear proteasome interacting proteins by quantitative analysis of proteasome complexes immunopurified from nuclei of U937 cells using the MCP21 antibody (targeting the α2 subunit of 20S proteasome), as described previously (31). As expected, all 20S proteasome and 19S regulatory complex subunits, as well as known proteasome interactors, such as PA28γ, PA200, and USP14, were found in this category [abundance ratios (IP 20S/IP control) above 2 and *P* value below 0.05 ($n = 3$)] (*SI Appendix*, Fig. S2*A* and Dataset S4). Interestingly, the protein FAM192A showed an enrichment factor of 6.4 and a *P* value $<5 \times 10^{-4}$ and thus clearly qualifies as a proteasome interacting protein.

Further quantitative analysis of proteasome-associated proteins in HeLa cells showed that FAM192A is recruited on proteasomes in a PA28γ-dependent manner (Fig. 1*D*), because it is absent in proteasome immunoprecipitates after PA28γ knockdown. The enrichment in anti-FAM192A immunoprecipitates of all subunits of the 19S regulatory complex (PSMCx and PSMDx) (*SI Appendix*, Fig. S2*B*) demonstrated that FAM192A is also recruited on hybrid proteasomes, most likely via its interaction with PA28γ.

Interestingly, these experiments also showed that co-IP of PA28γ with 20S proteasome was halved ($P = 0.02$) in siRNA FAM192A-depleted cells (Fig. 1*D*). This result was confirmed by reverse anti-PA28γ co-IP experiments using wild-type and FAM192A$^{-/-}$ U2OS cell extracts, showing that indeed FAM192A depletion elicits a twofold decrease in PA28γ/α4 interaction (Fig. 1*E*). Thus, FAM192A promotes the association of PA28γ with the 20S proteasome.

Altogether, our experiments establish that FAM192A is a major direct interactor of PA28γ, recruited to proteasome complexes via PA28γ and favoring the association of PA28γ with the 20S proteasome. FAM192A is also called NIP30 (NEFA-interacting protein 30 kD), which might refer to a NIP-(4-hydroxy-5-iodo-3-nitrophenyl acetate) labeled 30-kD protein that interacts with phosphatidylinositol biphosphate (34). Based on the above experiments, and since FAM192A has no clear assigned cellular function, we propose to rename it PIP30, for PA28γ interacting protein 30 kDa. This name will be used thereafter in this report.

PA28γ/PIP30 Interaction Is Stabilized by CK2 Phosphorylation of PIP30 C Terminus. Evolutionary analyses show that the PIP30 sequence is characterized by the presence of three conserved domains: an N-terminal signature domain (pfam10187, also called NIP30 domain, ∼100 amino acids) and two smaller motifs (*SI Appendix*, Fig. S3*A*). The pfam10187 domain is found in metazoa as well as in all major eukaryotic supergoups. This allows tracing back the PIP30 gene to early stages of eukaryote evolution (*SI Appendix*, Fig. S3*B*), as it is the case for PA28γ (4). The conserved C-terminal motifs of PIP30 proteins are enriched in phosphorylatable residues, including a completely conserved tyrosine and several serine residues (*SI Appendix*, Fig. S3*A*).

Using various truncation mutants, we determined that the last 54 amino acids of PIP30 (amino acids 201–254; i.e., the H201 mutant) are necessary and sufficient for interaction with endogenous PA28γ and that amino acids 223–230 are critical for the association (Fig. 2*A* and *SI Appendix*, Fig. S4 *A* and *B*). This C-terminal region includes the highly conserved serine-rich and acidic sequence highlighted in *SI Appendix*, Fig. S3*A* and contains two SDSE motifs (*SI Appendix*, Fig. S4*C*) that both match the canonical consensus site (S/T-X-X-E/D/pS/pT) for casein kinase 2 (CK2) (35, 36). Indeed, we found that this region can be phosphorylated by CK2 in vitro (Fig. 2*B*). Phosphorylation is dependent on the integrity of the CK2 consensus sites, as it was reduced when the serine residues S_{222} and S_{228} were replaced by alanine (mutant SS-AA), and abolished or strongly impaired when the acidic residues within the two CK2 consensus motifs were converted into basic lysine residues (mutants $D_{223}E_{225}$-KK and $D_{229}E_{231}$-KK, respectively) (Fig. 2*B*).

In cells, in the context of the full-length GFP-PIP30 protein (Fig. 2*C* and *SI Appendix*, Fig. S4*D*), like in vitro with the C-terminal part of PIP30 (*SI Appendix*, Fig. S4*E*), these mutations altered the binding to PA28γ. In a manner parallel to their effects on CK2 phosphorylation in vitro, the acidic mutants abolished or strongly impaired the binding to PA28γ, while the SS-AA mutant reduced it (Fig. 2*C* and *SI Appendix*, Fig. S4*E*). The weaker binding of the SS-AA mutant strongly suggests that phosphorylation is stabilizing PA28γ/PIP30 interaction. Indeed, when using purified proteins, PA28γ showed more affinity for CK2-phosphorylated than for nonphosphorylated PIP30 (Fig. 2*D*).

To verify that CK2 is the endogenous kinase phosphorylating PIP30, we treated cells with the selective CK2 inhibitor CX-4945 (37). This treatment revealed a second, faster-migrating band (Fig. 2*E*), suggesting that in cells PIP30 is primarily in a CK2-phosphorylated form. This conclusion is strengthened by thorough

CELL BIOLOGY

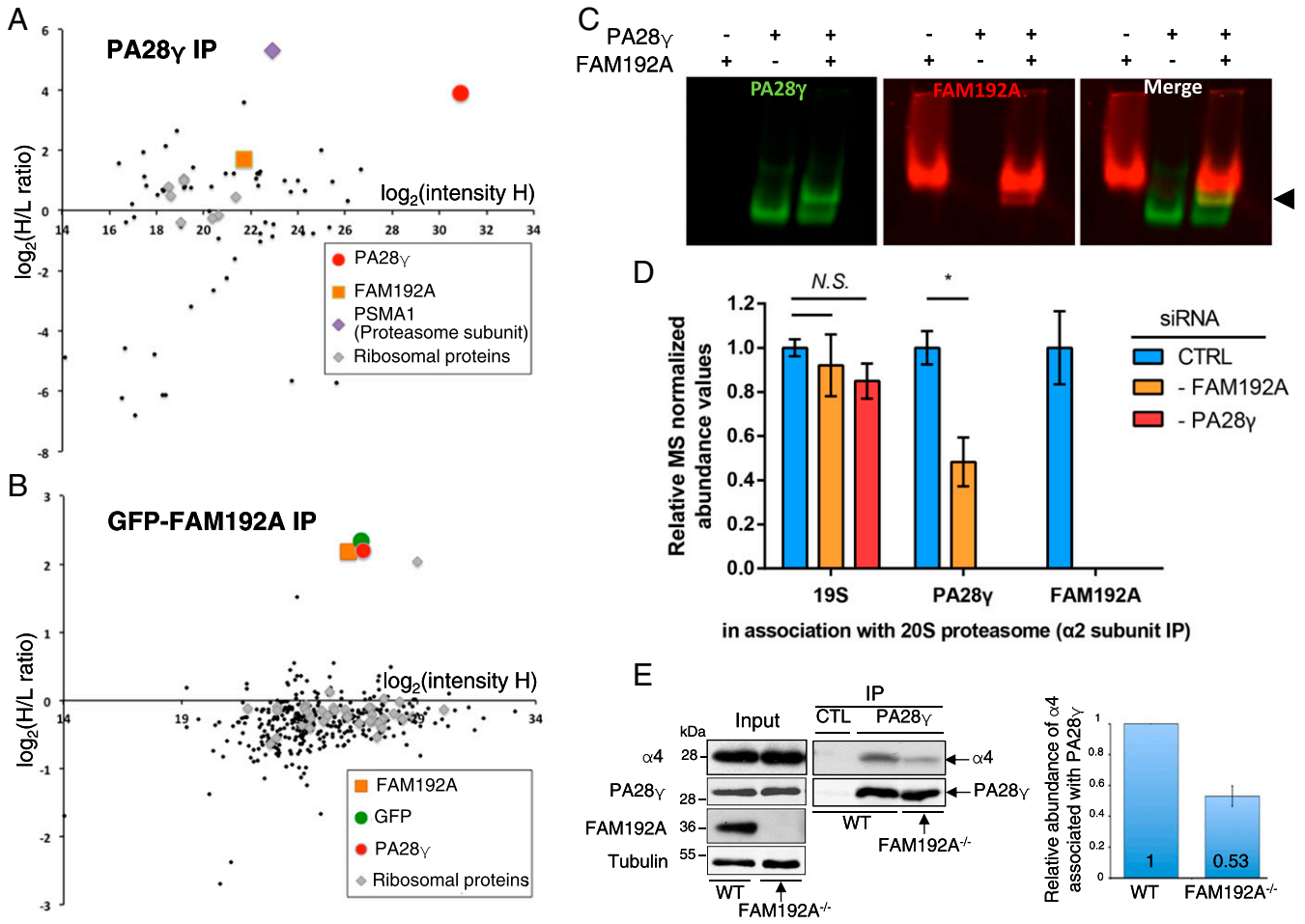

Fig. 1. FAM192A is a direct interactor of PA28γ that increases 20S proteasome/PA28γ interaction. (*A*) Graphic representation of the result of endogenous PA28γ SILAC IP in U2OS cells, visualized by plotting $\log_2$(H/L) vs. $\log_2$(H intensity) values for all 68 human protein groups quantified by MaxQuant, with a minimum of two unique peptides identified. Proteins specifically interacting with the bait (i.e., PA28γ) are expected to show H/L ratios higher than 1. In contrast, proteins non-specifically binding to the beads (experimental contaminants) are expected to show H/L ratios close to 1. Proteins with ratios lower than 1 are mostly environmental contaminants, such as keratins. (*B*) Graphic representation of the result of the SILAC GFP-TRAP IP of GFP-FAM192A, visualized by plotting $\log_2$(H/L) vs. $\log_2$(H intensity) values for all 364 protein groups quantified by MaxQuant with a minimum of two unique peptides identified. In both graphs, PA28γ is indicated by a red dot, FAM192A is indicated by an orange square, and GFP by a green dot. The PSMA1 subunit of the 20S core proteasome is indicated by a violet diamond. Ribosomal proteins, which can be considered here as nonspecific interaction partners, are indicated by gray diamonds. (*C*) Recombinant PA28γ and FAM192A directly interact with each other, as analyzed by native electrophoresis. After electrophoresis, the proteins were transferred on membrane and immunoprobed with specific antibodies visualized with an Odyssey infrared imaging system (LI-COR Biosciences). The arrowhead on the right indicates the formation of a complex (yellow) between purified PA28γ (green) and PIP30 (red). (*D*) Effect of FAM192A or PA28γ knockdown on the incorporation of 19S, PA28γ, and FAM192A into proteasome complexes. Proteasome complexes were immunopurified using the MCP21 antibody (targeting the α2 subunit of 20S proteasome) from total extracts of siRNA-treated HeLa cells. Proteins were identified and quantified by nano–LC-MS/MS analysis. For each analyzed sample, a quantification value was calculated by averaging XIC (i.e., eXtracted Ion Chromatogram) area signals of all of the proteospecific peptides identified from subunits of each regulator (19S, PA28γ, FAM192A) associated with the 20S proteasome. The same quantification value was computed for the noncatalytic subunits of the 20S proteasome and used to normalize the abundance of the 19S, PA28γ, and FAM192A regulators in each sample. Then, the values obtained for three biological replicates were normalized (control set to 1 for each regulator) for graphical representation. SD were calculated from triplicates. Statistical analysis was performed using a two-sample Student's *t* test assuming unequal variances. N.S., nonsignificant; $*P = 0.02$. (*E*) Quantification of PA28γ-bound 20S proteasome in wild-type and FAM192A$^{-/-}$ U2OS cells, as determined by co-IP of α4 subunit from 150 μg of total cell extract with anti-PA28γ antibodies. The *Right* panel is constructed from three independent experiments (error bars: SD). CTL, control IgGs; CTRL, control.

analysis of the phosphorylated semitryptic PIP30 peptides found in our mass spectrometry analyses of anti-PIP30 immunoprecipitates (*SI Appendix*, Fig. S5). While only a minor fraction of endogenous PIP30 was nonphosphorylated in wild-type cells upon CK2 inhibition for 24 h, it was mainly non- or hypophosphorylated in PA28γ$^{-/-}$ cells after the same treatment (Fig. 2*E*). This finding suggests that, although PIP30 does not require PA28γ for being phosphorylated, the binding to PA28γ protects it from being dephosphorylated. This was confirmed by the fact that λ-phosphatase can dephosphorylate a fraction of immunoprecipitated endogenous PIP30, but not the endogenous PIP30 coimmunoprecipitated with PA28γ (*SI Appendix*, Fig. S4*F*). Finally, after CX-4945 treatment, only the phosphorylated PIP30 was retrieved upon PA28γ IP (Fig. 2*F*), showing that the phosphorylation of PIP30 by CK2 in cells stabilizes its interaction with PA28γ. Taken together, our results show that the C-terminal end of PIP30 protein is critical for its binding to PA28γ and that its phosphorylation by CK2 stabilizes this interaction.

PIP30 Controls Substrate Diffusion to the Catalytic Chamber of the Proteasome. We next assessed whether PIP30 could interfere with the best-known property of PA28γ: that is, its ability to activate the peptidase activities of the proteasome in vitro.

Using recombinant PIP30 in combination with PA28γ and the 20S proteasome, we found that PIP30 differentially altered

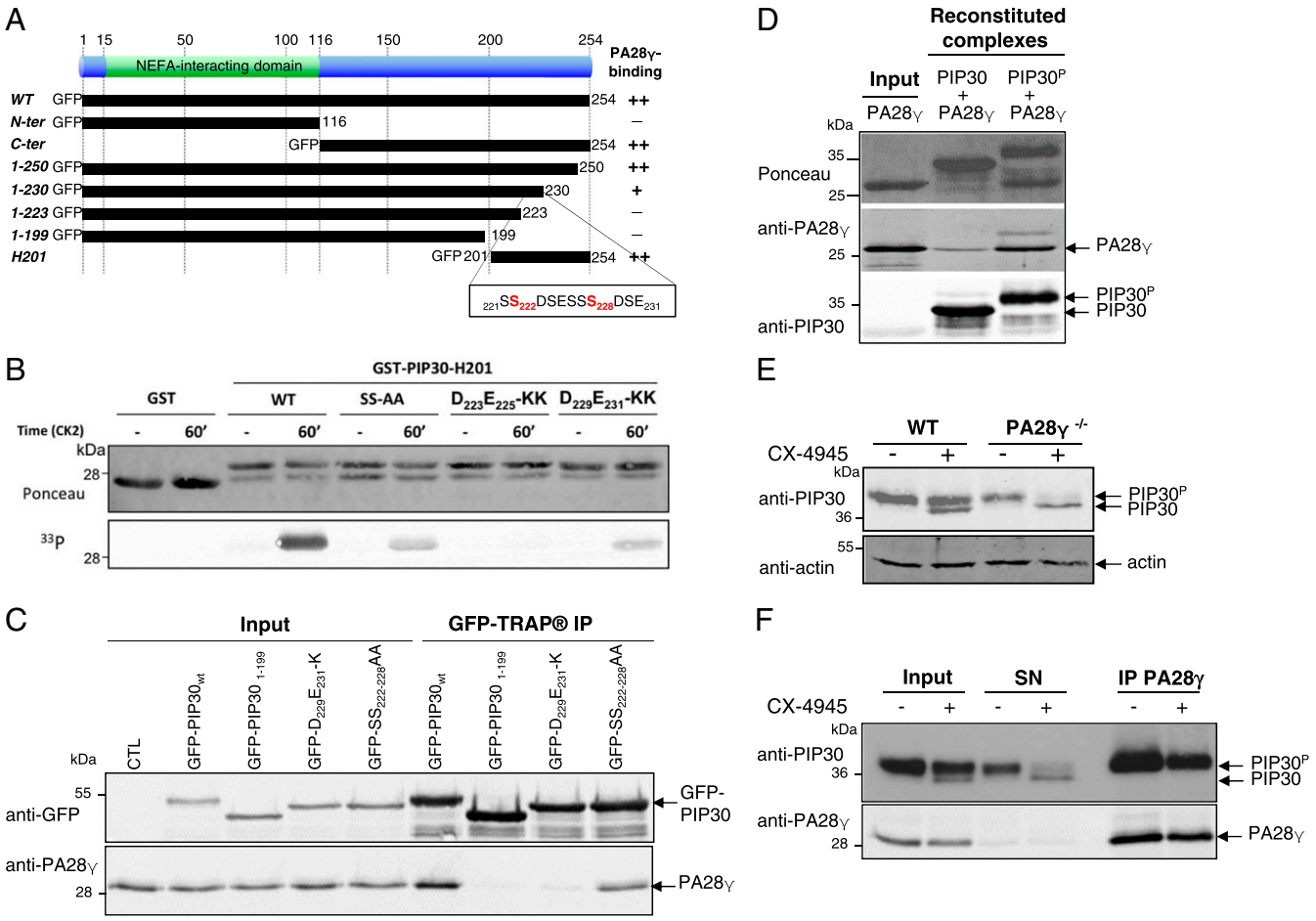

Fig. 2. PIP30 interacts with PA28γ via its CK2-phosphorylated C terminus. (*A*) Graphical summary of the analysis of the interaction between several GFP-PIP30 truncation mutants and PA28γ. (*B*) The C-terminal end of PIP30 (GST-PIP30-H201) is phosphorylated in vitro by CK2 and point mutations in its CK2 consensus sites strongly reduce its phosphorylation. Purified GST, GST-PIP30-H201, and GST-PIP30-H201 mutants were incubated with CK2, in the presence of [^{33}P]-ATP for the indicated times. The presence of GST-tagged proteins was revealed by Ponceau staining and their phosphorylation was detected by autoradiography. (*C*) Point mutations in the CK2 consensus motifs of GFP-PIP30 strongly reduce the interaction between GFP-PIP30 and PA28γ in cells. U2OS cells were transiently transfected with wild-type or the indicated mutants of PIP30 fused to GFP. GFP-tagged proteins were pulled down using GFP-TRAP beads and the presence of coimmunoprecipitated PA28γ was assessed by Western blot. Wild-type GFP-PIP30 was used as a positive control and GFP-PIP30$_{1–199}$ mutant as a negative control. (*D*) PA28γ has more affinity for CK2-phosphorylated PIP30 (PIP30^{P}) than for unphosphorylated PIP30 in vitro. Bacterially expressed and purified His-PIP30 was either phosphorylated, or not, by CK2 in vitro and then mixed with recombinant PA28γ. The complex was purified on a Ni-NTA column and analyzed by SDS/PAGE and Western blot with anti-His anti-PA28γ antibodies. (*E*) The association between PA28γ and PIP30 protects PIP30 from dephosphorylation. Wild-type and PA28γ$^{-/-}$ U2OS cells were either treated, or not, with CX-4945 (10 μM) for 24 h and the PIP30 PAGE migration profile was analyzed by Western blot. The phosphorylated form (PIP30^{P}) and the unphosphorylated form of PIP30 are indicated. (*F*) PA28γ interacts with the phosphorylated form of endogenous PIP30 in cells. Endogenous PA28γ was immunoprecipitated from 500 μg of total extracts from U2OS cells either treated, or not, with CX-4945 (10 μM) for 24 h. The presence of coimmunoprecipitated PIP30 was assessed by Western blot. The input and unbound (SN) fractions were also analyzed. After CX-4945 treatment, two bands appear for endogenous PIP30, the phosphorylated form (PIP30^{P}) and the unphosphorylated form (PIP30), as indicated. CTL, untransfected cells.

degradation of a panel of standard proteasome peptide substrates (38) by the PA28γ-activated proteasome (Fig. 3*A*). For example, while the activation of Suc-LLVY-amc (LLVY) and Ac-nLPnLD-amc (nLPnLD) degradation was partially inhibited, degradation of Boc-LRR-amc (LRR) was essentially insensitive to the presence of PIP30 (Fig. 3*A* and *SI Appendix*, Fig. S6*A*). The lack of effect of PIP30 on LRR degradation shows that its negative effects on other peptides is not due to alteration of the stability of the 20S proteasome/PA28γ complex, since the proteasome remains fully activated in this case. Importantly, PIP30 had no effect when PA28αβ was used to activate the 20S proteasome or after mutations that prevent its binding to PA28γ (*SI Appendix*, Fig. S6*B*). This establishes that the effects of PIP30 on proteasome activities, described in this report, are not direct but require its interaction with PA28γ, even though it remains formally possible that PIP30 could nevertheless also affect proteasome functions through undetected labile or transient interactions independent from PA28γ. The differential effects of PIP30 were not correlated with specific proteasome peptidase activities (Fig. 3*A*), suggesting that the effects of PIP30 are not a result of alteration of the proteasome active sites. To confirm this hypothesis, we used the proteasome activity probe Bodipy TMR-Ahx$_3$L$_3$VS (a generous gift of Huib Ovaa, Leiden University, Leiden, The Netherlands), which labels efficiently the β2 (trypsin-like activity) and β5 (chymotrypsin-like activity) subunits of the proteasome (39, 40). We found that the ratio between β2 and β5 labeling was not altered by PIP30 (Fig. 3*B*), showing that the relative activity of both sites is not changed. Therefore, the differential degradation of LRR (β2 substrate) and LLVY (β5 substrate) elicited by PIP30 is most likely due to a differential

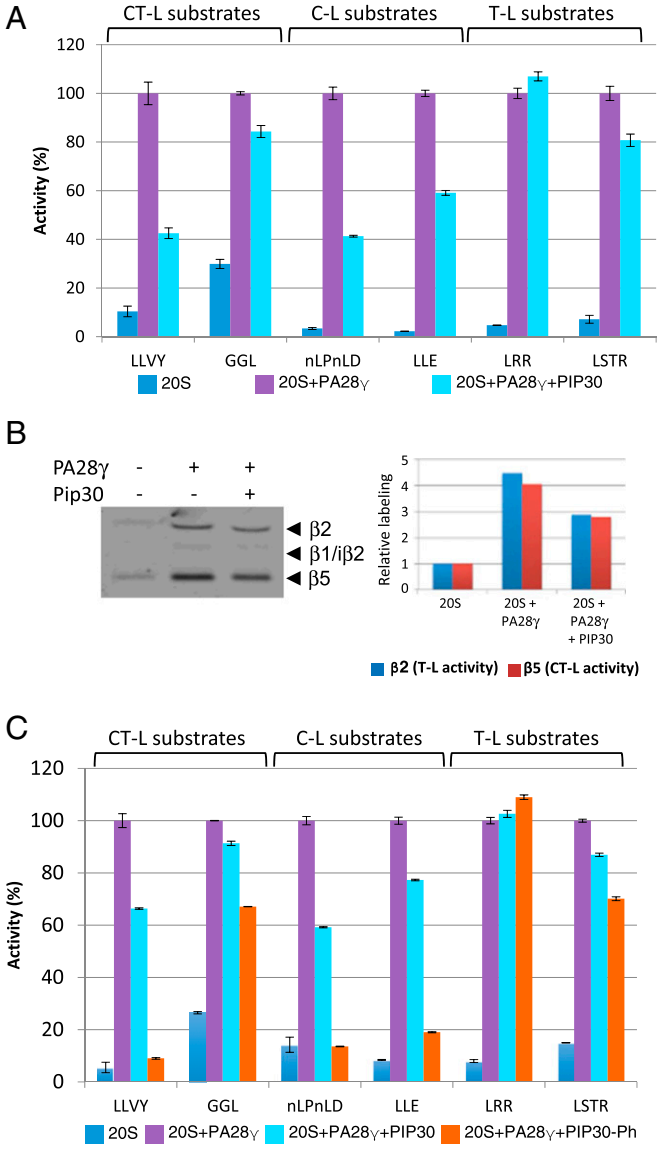

Fig. 3. PIP30 differentially affects peptide diffusion toward the catalytic chamber of the proteasome. (*A*) Inhibition by PIP30 of PA28γ-activated 20S proteasome is peptide substrate-specific. Proteasome activity was assayed in the presence of the indicated peptides and proteins and normalized by setting to 100% the value obtained in the presence of 20S proteasome and PA28γ. The assays were performed for 20 min at 37 °C in a 50-μL reaction mixture containing the indicated combinations of 20S proteasome (0.5 μg), PA28γ (1 μg), and PIP30 (4 μg). The respective final concentrations of the 20S proteasome and PA28γ are set up such as the peptidase activities are not fully activated (i.e., PA28γ is limiting in the assay). At the final concentration used for PIP30, the inhibitory effect is maximal (*SI Appendix*, Fig. S6*A*). Error bars represent deviation from the mean of technical duplicates. The figure is representative of more than three distinct experiments. Peptides used are substrates of the following peptidase activities of the 20S proteasome: Suc-LLVY-amc, Z-GGL-amc: chymotrypsin-like activity; Ac-nLPnLD-amc, Z-LLE-amc: caspase-like activity; Boc-LRR-amc, Boc-LSTR-amc: trypsin-like activity. (*B*) The activity of the chymotrypsin-like and trypsin-like catalytic sites of the 20S proteasome is not modified by PIP30: 20S proteasome (2 μg) was mixed in reaction buffer (Tris·HCl 20 mM pH 7.5, DTT 1 mM, glycerol 10%) in a final volume of 18 μL, with either no protein or with PA28γ (6 μg) preincubated for 5 min at room temperature with or without PIP30 (8.3 μg). After incubation 5 min at room temperature, 2 μL of the probe Bodipy TMR-Ahx$_3$L$_3$VS (1 μM in reaction buffer) were added to each sample and the mixtures were further incubated 15 min at 37 °C. After denaturation with Laemmli buffer and electrophoresis, the labeled proteasome subunits were visualized (*Left*) using a Typhoon FLA 7000 (GE Healthcare). The labeling of subunits β2 and β5 was quantified and plotted after normalization by the value of their labeling in 20S proteasome alone (*Right*). In the experimental conditions used, the labeling of both subunits is roughly proportional to their activity. The figure is representative of three distinct experiments. (*C*) Comparison of the effects of PIP30 and its CK2-phosphorylated form (PIP30-Ph) on the peptidase activities of the PA28γ/20S proteasome complex. The experiments were performed as in *A*, except that only 2 μg of PIP30 and PIP30-Ph were used per assay. Error bars represent deviation from the mean of technical duplicates. The figure is representative of three distinct experiments. C-L, caspase-like; CT-L, chymotrypsin-like; T-L, trypsin-like.

diffusion rate into the catalytic chamber of the proteasome. This strongly suggests that PIP30 regulates peptide entrance or transit through the channel opened by PA28γ upon binding to the 20S proteasome.

We next assessed whether PIP30 phosphorylation affects its effect on peptide degradation. Comparing nonphosphorylated and CK2-phosphorylated PIP30 (*SI Appendix*, Fig. S10*D*), we found that phosphorylation of PIP30 enhanced its inhibitory effects (Fig. 3*C*). For the most affected peptides, phosphorylated PIP30 was able to abrogate the activating effect of PA28γ on their hydrolysis. However, it had a limited effect on other peptides and remained without effect on the basic LRR substrate (Fig. 3*C*).

Overall, these data show that PIP30 is able to alter the 20S proteasome-activating properties of PA28γ in vitro. In this process, it seems to act as a phosphorylation-modulated filter that differentially impairs the entrance or the transit of peptide substrates through the PA28γ channel.

PIP30 Alters PA28γ Functions in CB Dynamics. We have previously shown that PA28γ overexpression leads to the disruption of CBs (21), which are evolutionary conserved coilin-dependent and coilin-rich subnuclear compartments. CBs are involved in the maturation of small nuclear ribonucleoproteins (RNPs) and small nucleolar RNPs, as well as in the processing of histone pre-mRNAs (41, 42). We thus tested whether PIP30 has also a role in CB dynamics. First, we compared CB number in wild-type, PA28γ$^{-/-}$, and PIP30$^{-/-}$ U2OS cells. We found that while 80% of wild-type and PA28γ$^{-/-}$ U2OS cells display CBs, only 40% of PIP30$^{-/-}$ cells are CB^{+} (Fig. 4 *A* and *B*). Furthermore, in cells displaying CBs, the absence of PIP30 leads to a decrease in the average number of CBs per nucleus (Fig. 4*C*). The effect of PIP30 depletion was rescued by expression of GFP-PIP30 (Fig. 4*D*). Furthermore, the PIP30 mutants impaired in their binding to PA28γ (i.e., GFP-PIP30$_{1–199}$, D$_{223}$E$_{225}$-KK, and D$_{229}$E$_{231}$-KK) did not significantly rescue the phenotype, compared with GFP alone (Fig. 4*D*). Together, these results show that PIP30, like PA28γ (21), controls the steady-state number of CBs and that this depends on its binding to PA28γ. However, PIP30 and PA28γ do not have the same effects in this process. An important question was to assess whether the effect of PIP30 depletion is dependent upon the presence in cells of PA28γ. We thus compared the effect of PIP30 knockdown in wild-type and PA28γ$^{-/-}$ cells (Fig. 4*E*). The results show that in both cell lines depletion of PIP30 entails a decrease in the number of cells with CBs. However, the effect of PIP30 depletion seems less drastic in PA28γ$^{-/-}$ compared with wild-type cells. Together, these results suggest two components in the functions of PIP30 in CB dynamics: one critical that is PA28γ-dependent, and another that is PA28γ-independent.

In the absence of PIP30 (i.e., in siRNA PIP30-depleted or PIP30 knockout cells, but not in control cells) we observed an accumulation of PA28γ in all residual CBs, either identified by coilin (Fig. 5*A*) or WRAP53 (another CB marker) staining (*SI Appendix*, Fig. S7*A*). Furthermore, reexpression of GFP-PIP30 in PIP30-depleted cells abrogated the accumulation of PA28γ in CBs (*SI Appendix*, Fig. S7*B*). These observations demonstrate that PIP30 inhibits PA28γ subnuclear localization in CBs.

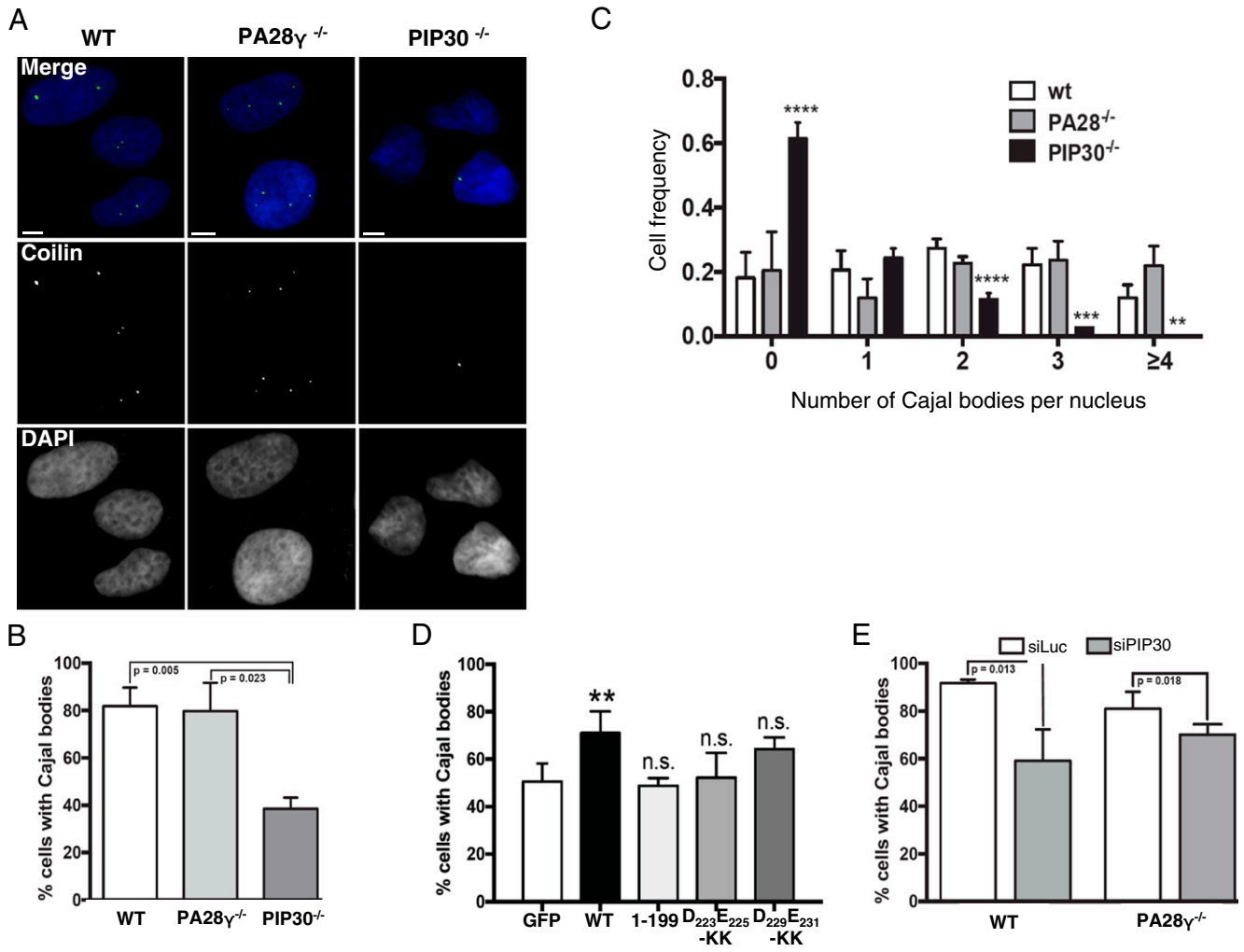

Fig. 4. PIP30 is involved in CB dynamics. (*A*) PA28γ and PIP30 depletion have differential effects on CB dynamics. The presence of CBs in wild-type, PA28γ$^{-/-}$, and PIP30$^{-/-}$ U2OS cells was analyzed by indirect immunofluorescence using 5P10 anticoilin antibody. (Scale bars, 10 μm.) (*B*) The coilin signal was used to determine the percentage of CB^{+} cells for wild-type, PA28γ$^{-/-}$, and PIP30$^{-/-}$ U2OS cells. Data represent the means and SD from three independent experiments (n = 759 wild-type, 822 PA28γ $^{-/-}$, and 842 PIP30 $^{-/-}$ cells; n > 230 cells per condition per experiment). Two-tailed paired t tests showed a significant difference of PIP30$^{-/-}$ vs. wild-type U2OS cells (P = 0.005). (*C*) PIP30 depletion induces a decrease in the mean number of CBs per nucleus. The coilin signal was used to quantify the number of CBs per nucleus in wild-type, PA28γ$^{-/-}$, and PIP30$^{-/-}$ U2OS cells. Data show the percentage of cells displaying 0, 1, 2, 3, or more CBs per nucleus and represent the mean and SD of three independent experiments (n > 250 cells per condition per experiment). Asterisks indicate CB frequencies significantly different between mutant and wild-type U2OS cells (multiple t tests): ****$P < 10^{-4}$; ***$P < 10^{-3}$; **$P < 10^{-2}$. (*D*) The overexpression of GFP-PIP30, but not of GFP-PIP30$_{1–199}$, GFP-PIP30 $D_{223}E_{225}$-KK, and GFP-PIP30 $D_{229}E_{231}$-KK mutants, defective for PA28γ binding, rescues the formation and stability of CBs in U2OS PIP30$^{-/-}$ cells. PIP30$^{-/-}$ cells were transfected with 100 ng of GFP, GFP-PIP30 wild-type, GFP-PIP30$_{1–199}$, GFP-PIP30 $D_{223}E_{225}$-KK, and GFP-PIP30 $D_{229}E_{231}$-KK plasmids. The percentage of CB^{+} cells was manually determined in each condition by analyzing the presence/absence of coilin dots in all GFP^{+} cells (n > 30 transfected cells per condition per experiment). ANOVA analysis of four independent experiments showed significant differences among means (P = 0.0027). Only the GFP-PIP30 wild-type showed a significant difference with GFP (Dunnett's multiple comparison test, P = 0.0055). (*E*) The effect of PIP30 knockdown on CB dynamics is attenuated in PA28γ$^{-/-}$ cells. U2OS and PA28γ$^{-/-}$ cells were transfected with 50 nM siRNAs directed against luciferase (siLuc) and PIP30 (siPIP30), during 48 h. The percentage of CB^{+} cells was determined in each condition by analyzing the presence/absence of coilin dots in all cells. Data represent the means and SD from four independent experiments and were analyzed using paired two-tailed t tests (n > 280 cells per condition per experiment). n.s., nonsignificant.

Because PA28γ is known to bind to the key CB component coilin (21) (Dataset S2), we analyzed whether PIP30 could affect this process. We observed that PIP30 depletion led to an increased interaction of PA28γ with coilin, as seen by co-IP experiments (Fig. 5*B*). In line with this observation, in the absence of PIP30, an increased number of dots could be seen by PLA using anti-PA28γ and coilin antibodies, supporting the notion that PIP30 inhibits PA28γ/coilin interaction (*SI Appendix*, Fig. S8).

Altogether, these experiments show that PIP30 effect on CBs is mediated through its ability to bind PA28γ and to counteract PA28γ association with coilin, confirming that PIP30 indeed functions as an endogenous regulator of PA28γ.

Discussion

Despite the fact that PA28 complexes have long been known, little is understood regarding their roles as proteasome regulators, besides their ability to open upon binding the gated channel of the 20S proteasome. However, because specific protein substrates have been described for PA28γ, it is possible that these regulators are not just passively opening the gate of the 20S proteasome but somehow contribute to substrate selection and possibly unfolding and injection into the 20S core. If true, then it is likely that they work in synergy with other proteins, because by themselves they seem a priori unable to actively promote proteasomal

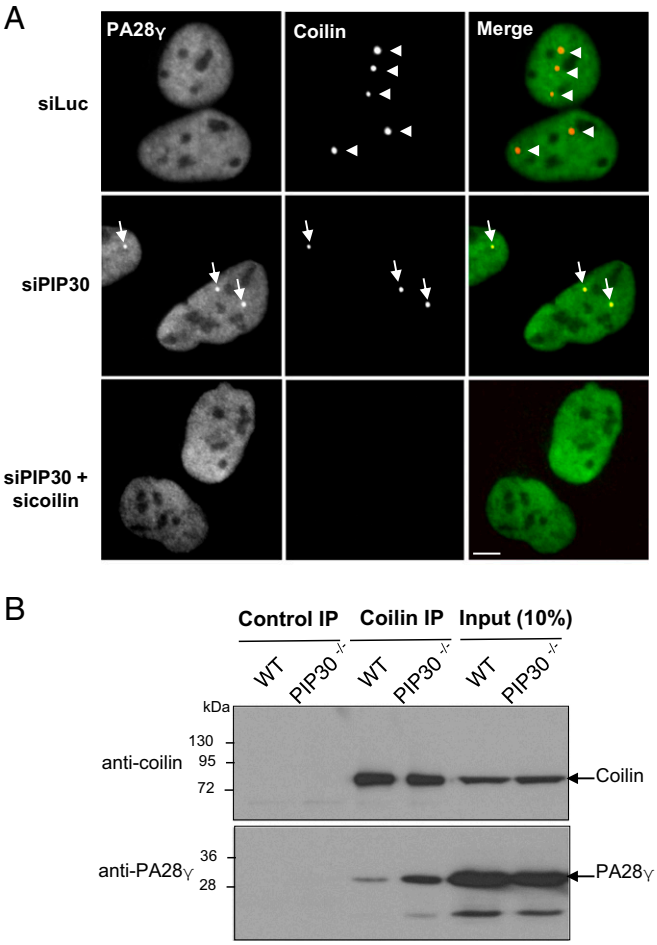

Fig. 5. PIP30 depletion induces accumulation of PA28γ in residual CBs and enhances the interaction of PA28γ with coilin. (*A*) PIP30 depletion induces PA28γ accumulation in CBs. The colocalization of endogenous PA28γ and coilin was analyzed by indirect immunofluorescence in U2OS cells treated either with a control siRNA (siLuc), a siRNA targeting PIP30, or siRNAs targeting both PIP30 and coilin. In the merge panels, the coilin signal is in red and the PA28γ signal in green. Arrowheads indicate CBs positive for coilin only, while arrows indicate CBs positive for both coilin and PA28γ. (Scale bars, 10 μm.) (*B*) PIP30 depletion increases the level of endogenous coilin coimmunoprecipitated with PA28γ. Nuclear cell extracts from asynchronously growing parental (wild-type) or PIP30$^{-/-}$ U2OS cells were incubated with control IgG or anti-coilin antibodies. Immunocomplexes were analyzed by SDS/PAGE, probed for the indicated proteins, and the amount of PA28γ associated with coilin was quantified and normalized to the amount of immunoprecipitated coilin. The figure is representative of three distinct experiments.

degradation of specific protein substrates. We thus performed various proteomics experiments to characterize proteins associated with PA28γ.

Among the interaction partners of endogenous PA28γ, we found several proteins involved in the regulation of RNA processing (Dataset S1), suggesting an important role of PA28γ in this function. Although PA28γ interacts with the 20S proteasome, we identified only the α6 subunit (PSMA1) in the conditions used. However, we found most 20S proteasome as well as 19S complex subunits with high H/L ratios when PA28γ pull-downs were performed with extracts of proteasome inhibitor-treated cells (Dataset S5), confirming both that (*i*) PA28γ/20S proteasome interaction is labile (31) and is stabilized upon proteasome inhibition (11, 43), and (*ii*) PA28γ, as this has been described for PA28αβ, can also be recruited in hybrid forms of the proteasome in which the 20S proteasome is bound to the 19S complex on one side and PA28γ on the other side.

Importantly, we identified a prominent partner of PA28γ, PIP30/FAM192A. Interaction between PIP30 and PA28γ has already been listed in large-scale proteomics experiment data in *Drosophila* and human (44, 45). However, our results validate its biological relevance.

We demonstrated that this interaction is direct and occurs in cells with 20S proteasome-free and -bound PA28γ. The interaction is specific for PA28γ because we found no interaction between PIP30 and PA28αβ in vitro. This suggests that the interaction may involve the homolog-specific insert, which is the most divergent domain between PA28 paralogs (46). Importantly we show that the PA28γ-binding region of PIP30 is located in its C-terminal end and that CK2 phosphorylation of a short motif in this region stabilizes its association with PA28γ. Because mutation of serine residues (S_{222} and S_{228}) of both typical CK2 targets does not completely abolish binding, it is likely that additional serine residues are phosphorylated by CK2. This is in line with the ability of CK2 to catalyze the generation of phosphoserine stretches (36), and in agreement with our proteomics analyses (*SI Appendix*, Fig. S5) and with the report that S_{219}, S_{221}, S_{222}, and S_{224} of PIP30 are phosphorylated in vivo [Global Proteome Machine, Accession: ENSP00000335808 (47)]. The role of these multiple phosphorylation events is not clear. CK2 is indeed a ubiquitous and pleiotropic kinase (48), and even if its activity has been shown to be positively regulated by the Wnt/β-catenin pathway (49) it is considered to be constitutively active in cells. Our results also suggest an extremely slow turnover of the phosphate groups for the majority of PIP30 bound to PA28γ, probably because steric hindrance makes them inaccessible to phosphatases once the complex is formed. It thus seems unlikely that CK2 phosphorylation of PIP30 is used in cells to dynamically control PIP30/PA28γ interaction.

Comparison of PIP30 and PA28γ distributions within the eukaryotic phylogenetic tree (*SI Appendix*, Fig. S3*B*) shows that their presence or absence is not correlated. For example, in all Ascomycota, including *Saccharomyces cerevisiae*, PIP30 is present while PA28γ has been lost. This indicates that the two proteins may function independently of each other. However, in human cells, more than 70% of PA28γ and PIP30/FAM192A are associated in the same complex (*SI Appendix*, Fig. S1*B*), suggesting that they cooperate in most of their functions.

In line with this assertion, our data show that PIP30 regulates the function of PA28γ as a proteasome regulator, since its invalidation halves the intracellular level of the PA28γ/20S proteasome complex (Fig. 1 *D* and *E*). However, because the 20S proteasome/PA28γ complex only represents ≤5% of the total 20S proteasome (29), it is difficult to predict the biological impact of this effect. Based on our in vitro analyses showing that PIP30 inhibits the degradation of some peptides by reconstituted 20S proteasome/PA28γ complexes but is permissive for others (Fig. 3), it is tempting to speculate that PIP30 acts as a molecular sieve that hinders entrance of some protein substrates into the PA28γ channel while being neutral for others. The likely binding of PIP30 to the PA28γ-specific insert that forms a loop located close to the pore of the complex (25, 50) is compatible with such a role. Confirmation and further dissection of this hypothesis requires comparison of proteasome- and PA28γ-dependent substrates whose degradation is differentially regulated by PIP30. Unfortunately, among the several described PA28γ substrates that we tested, only p21 degradation proved to be PA28γ-dependent in our conditions, and the cellular stability of this protein turned out to be insensitive to PIP30 presence or absence.

Interestingly, the notion that PA28 complexes could act as a molecular sieve has already been put forward for PA28αβ, based on detailed studies showing that it selectively filters peptide

products coming out of the proteasome (8, 51). This raises the possibility that PIP30 could, together with PA28γ, play a selective role not only on substrate entrance but also peptide release by the proteasome.

Taken together, our data are compatible with the interesting hypothesis that binding of PIP30 to PA28γ could induce a global conformational change of the latter that would both favor its binding to the 20S proteasome and alter its substrate selectivity through alteration of the entrance or the structure of its channel. Structure/functions analyses aiming at precisely mapping the consequences on PA28γ of PIP30 binding as well as detailed characterization of peptides produced by the proteasome in the presence of PA28γ and PA28γ/PIP30 complexes will help to answer these questions.

A second illustration of the role of PIP30 as a PA28γ regulator is the demonstration that both proteins intimately cooperate in the regulation of CB integrity. Indeed, PIP30 depletion leads to a strong decrease in the number of CBs and to an increased interaction between coilin and PA28γ (Fig. 5*B* and *SI Appendix*, Fig. S8 *A* and *B*). This mimics the phenotype induced by PA28γ overexpression (21) (Dataset S2). PIP30 depletion also elicits the accumulation of PA28γ in residual CBs, while PA28γ is usually not detectable in these structures. To our knowledge, PA28γ has only been observed in CBs of motor neurons from patients with type I spinal muscular atrophy (52). In these pathologic neurons, the assembly of CBs is impaired, due to the lack of the survival motor neuron protein, an essential CB component (53–55). Because CBs are dynamic structures undergoing constant remodeling (56), the accumulation of PA28γ in residual CBs observed in both PIP30$^{-/-}$ cells and spinal muscular atrophy motor neurons could reflect the fact that these residual CBs are stalled at transient intermediate stages of assembly/disassembly in which PA28γ is involved. Alternatively, the absence of PIP30 may result in the formation of defective CB structures that are not normally present in wild-type cells. Interestingly, the proteasome is not recruited into CBs, together with PA28γ, in the absence of PIP30 (*SI Appendix*, Fig. S9*A*), and proteasome inhibition—which greatly enhances the binding of PA28γ to the 20S core (11)—inhibits the accumulation of PA28γ into CBs (*SI Appendix*, Fig. S9*B*). These observations raise the possibility that the functions of PA28γ and PIP30 in CBs could be proteasome-independent.

Taking these data together, the effects of PIP30 deletion on CB integrity suggest that increasing the levels of PA28γ/coilin complexes negatively regulates the number of CBs and that PIP30 inhibits the association between PA28γ and coilin. This model supports the idea that PA28γ overexpression leads to CB destabilization by overwhelming PIP30 inhibition, and therefore that the equilibrium between free PA28γ and PIP30-bound PA28γ is an important parameter in this process. In this regard, it is interesting to note that CB fragmentation upon UV-C treatment is associated with the concomitant increase in PA28γ and its recruitment to coilin (21). If PIP30 levels are limiting in cells, the resulting excess of PIP30-free PA28γ might be sufficient to interact with coilin and induce CB fragmentation. However, as it is difficult to imagine that PA28γ functions in CBs could be taken in charge only by neosynthesized PA28γ that would have escaped definitive PIP30 inhibition, it seems more likely that the binding of PIP30 to PA28γ can be negatively regulated to favor their dissociation when needed. As mentioned above, our data do not support the idea that such regulation could be mediated only by modulation of CK2 activity or by dephosphorylation of CK2 sites on PIP30. Therefore, we speculate that other regulatory mechanisms, that are yet to be discovered, must be at play to dissociate the PA28γ/PIP30 complex. Because the interaction zone between PIP30 and PA28γ is protected against phosphatases, destabilization of the interaction is likely to occur through conformational changes incompatible with further binding. In principle, such conformational changes could be mediated by posttranslational modifications of either PA28γ or PIP30, or by binding of additional partners or chaperones able to alter upon binding the structure of the complex. Additional work is required to clarify this issue.

Taken together, the results presented here show that PIP30 is an important partner of PA28γ that regulates its interactome and therefore its functions, for example, by stabilizing its interaction with the 20S proteasome and inhibiting its interaction with coilin. Although most of the data presented in this report show an inhibitory role of PIP30 toward PA28γ functions, the fact that PIP30 does not influence the PA28γ-dependent degradation of the protein p21 shows that PIP30 is not a general inhibitor of PA28γ. In any case, because most PA28γ is bound to PIP30 in standard cell culture conditions, it is clear that PIP30 must now be taken into account when studying PA28γ. Although much remains to be understood regarding PIP30 biological functions, our results represent a significant breakthrough because they provide clues on the regulation of PA28γ/20S proteasome complex, as well as angles of attack to dissect PA28γ functions and mechanisms of action.

ACKNOWLEDGMENTS. The authors thanks Huib Ovaa (University of Leiden) for proteasome activity probes; Dr. Anne Blangy (Centre de Recherche en Biologie Cellulaire de Montpellier) for critical reading; the rotation students who participated to this work, including Pierre Bercier, Laure Dutrieux, Maryne Franceschi, Jean-Yves Frayssinhes, Anaïs Lugagne, Valentin Pineau, and Haifa Tlaiss; and the imaging facility MRI, member of the national infrastructure France-BioImaging supported by the French National Research Agency (ANR-10-INBS-04, "Investments for the future"). This work was supported by the CNRS, and by funding from the People Programme (Marie Curie Actions) of the EU Seventh Framework Programme FP7 REA agreement 290257, "UPStream" (to O.C.); the comité du Gard de la Ligue Nationale Contre le Cancer, Contract 158484 (to O.C.); the Association pour la Recherche sur le Cancer ARC PJA 20141201831 and SFI20111203984 (to S.B.); the Wellcome Trust, Grants 097945/B/11/Z and 108058/Z/15/Z (to A.I.L.); and the French Ministry of Research (Investissements d'Avenir Program, Proteomics French Infrastructure, ANR-10-INBS-08) and the Fonds Européens de Développement Régional, Toulouse Métropole, Région Occitanie (fellowships to T.M. and B.F.) to O.B.-S. Support to B.J.-N. was provided by the Marie Curie International Training Network "UPStream." S.B. was initially supported by European Molecular Biology Organization and Human Frontier Science Program Long Term Fellowships. This article is based upon work from European Cooperation in Science and Technology (COST) Action (PROTEOSTASIS BM1307), supported by COST.

1. Schmidt M, Finley D (2014) Regulation of proteasome activity in health and disease. *Biochim Biophys Acta* 1843:13–25.
2. Finley D, Chen X, Walters KJ (2016) Gates, channels, and switches: Elements of the proteasome machine. *Trends Biochem Sci* 41:77–93.
3. Collins GA, Goldberg AL (2017) The logic of the 26S proteasome. *Cell* 169: 792–806.
4. Fort P, Kajava AV, Delsuc F, Coux O (2015) Evolution of proteasome regulators in eukaryotes. *Genome Biol Evol* 7:1363–1379.
5. Zhang Z, et al. (1999) Proteasome activator 11S REG or PA28: Recombinant REG alpha/REG beta hetero-oligomers are heptamers. *Biochemistry* 38:5651–5658.
6. Huber EM, Groll M (2017) The mammalian proteasome activator PA28 forms an asymmetric $\alpha_4\beta_3$ complex. *Structure* 25:1473–1480.e3.
7. Preckel T, et al. (1999) Impaired immunoproteasome assembly and immune responses in PA28-/- mice. *Science* 286:2162–2165.
8. Cascio P (2014) PA28αβ: The enigmatic magic ring of the proteasome? *Biomolecules* 4: 566–584.
9. Wilk S, Chen WE, Magnusson RP (2000) Properties of the nuclear proteasome activator PA28gamma (REGgamma). *Arch Biochem Biophys* 383:265–271.
10. Mao I, Liu J, Li X, Luo H (2008) REGgamma, a proteasome activator and beyond? *Cell Mol Life Sci* 65:3971–3980.
11. Welk V, et al. (2016) Inhibition of proteasome activity induces formation of alternative proteasome complexes. *J Biol Chem* 291:13147–13159.
12. Chen X, Barton LF, Chi Y, Clurman BE, Roberts JM (2007) Ubiquitin-independent degradation of cell-cycle inhibitors by the REGgamma proteasome. *Mol Cell* 26: 843–852.
13. Li X, et al. (2007) Ubiquitin- and ATP-independent proteolytic turnover of p21 by the REGgamma-proteasome pathway. *Mol Cell* 26:831–842.
14. Kobayashi T, Wang J, Al-Ahmadie H, Abate-Shen C (2013) ARF regulates the stability of p16 protein via REGγ-dependent proteasome degradation. *Mol Cancer Res* 11: 828–833.
15. Zhang Z, Zhang R (2008) Proteasome activator PA28 gamma regulates p53 by enhancing its MDM2-mediated degradation. *EMBO J* 27:852–864.

16. Murata S, et al. (1999) Growth retardation in mice lacking the proteasome activator PA28gamma. *J Biol Chem* 274:38211–38215.
17. He J, et al. (2012) REGγ is associated with multiple oncogenic pathways in human cancers. *BMC Cancer* 12:75.
18. Chen D, Yang X, Huang L, Chi P (2013) The expression and clinical significance of PA28 γ in colorectal cancer. *J Investig Med* 61:1192–1196.
19. Li L, et al. (2015) REGγ is critical for skin carcinogenesis by modulating the Wnt/β-catenin pathway. *Nat Commun* 6:6875.
20. Zannini L, et al. (2008) REGgamma proteasome activator is involved in the maintenance of chromosomal stability. *Cell Cycle* 7:504–512.
21. Cioce M, Boulon S, Matera AG, Lamond AI (2006) UV-induced fragmentation of Cajal bodies. *J Cell Biol* 175:401–413.
22. Baldin V, et al. (2008) A novel role for PA28gamma-proteasome in nuclear speckle organization and SR protein trafficking. *Mol Biol Cell* 19:1706–1716.
23. Zannini L, Buscemi G, Fontanella E, Lisanti S, Delia D (2009) REGgamma/PA28gamma proteasome activator interacts with PML and Chk2 and affects PML nuclear bodies number. *Cell Cycle* 8:2399–2407.
24. Levy-Barda A, et al. (2011) Involvement of the nuclear proteasome activator PA28γ in the cellular response to DNA double-strand breaks. *Cell Cycle* 10:4300–4310.
25. Knowlton JR, et al. (1997) Structure of the proteasome activator REGalpha (PA28alpha). *Nature* 390:639–643.
26. Glickman MH, Coux O (2001) Purification and characterization of proteasomes from *Saccharomyces cerevisiae*. *Curr Protoc Protein Sci* Chapter 21:Unit 21.5.
27. Le Feuvre AY, Dantas-Barbosa C, Baldin V, Coux O (2009) High yield bacterial expression and purification of active recombinant PA28alphabeta complex. *Protein Expr Purif* 64:219–224.
28. Boulon S, et al. (2010) Establishment of a protein frequency library and its application in the reliable identification of specific protein interaction partners. *Mol Cell Proteomics* 9:861–879.
29. Fabre B, et al. (2014) Label-free quantitative proteomics reveals the dynamics of proteasome complexes composition and stoichiometry in a wide range of human cell lines. *J Proteome Res* 13:3027–3037.
30. Fabre B, et al. (2015) Deciphering preferential interactions within supramolecular protein complexes: The proteasome case. *Mol Syst Biol* 11:771.
31. Fabre B, et al. (2013) Subcellular distribution and dynamics of active proteasome complexes unraveled by a workflow combining in vivo complex cross-linking and quantitative proteomics. *Mol Cell Proteomics* 12:687–699.
32. ten Have S, Boulon S, Ahmad Y, Lamond AI (2011) Mass spectrometry-based immunoprecipitation proteomics–The user's guide. *Proteomics* 11:1153–1159.
33. Waddell DS, et al. (2016) Isolation, expression analysis and characterization of NEFA-interacting nuclear protein 30 and RING finger and SPRY domain containing 1 in skeletal muscle. *Gene* 576:319–332.
34. Slomiany A, Grabska M, Slomiany BL (2006) Homeostatic restitution of cell membranes. Nuclear membrane lipid biogenesis and transport of protein from cytosol to intranuclear spaces. *Int J Biol Sci* 2:216–226.
35. Meggio F, Pinna LA (2003) One-thousand-and-one substrates of protein kinase CK2? *FASEB J* 17:349–368.
36. Cesaro L, Pinna LA (2015) The generation of phosphoserine stretches in phosphoproteins: Mechanism and significance. *Mol Biosyst* 11:2666–2679.
37. Pierre F, et al. (2011) Discovery and SAR of 5-(3-chlorophenylamino)benzo[c][2,6] naphthyridine-8-carboxylic acid (CX-4945), the first clinical stage inhibitor of protein kinase CK2 for the treatment of cancer. *J Med Chem* 54:635–654.
38. Kisselev AF, Goldberg AL (2005) Monitoring activity and inhibition of 26S proteasomes with fluorogenic peptide substrates. *Methods Enzymol* 398:364–378.
39. Verdoes M, et al. (2006) A fluorescent broad-spectrum proteasome inhibitor for labeling proteasomes in vitro and in vivo. *Chem Biol* 13:1217–1226.
40. Berkers CR, et al. (2007) Profiling proteasome activity in tissue with fluorescent probes. *Mol Pharm* 4:739–748.
41. Morris GE (2008) The Cajal body. *Biochim Biophys Acta* 1783:2108–2115.
42. Trinkle-Mulcahy L, Sleeman JE (2016) The Cajal body and the nucleolus: "In a relationship" or "It's complicated"? *RNA Biol* 14:739–751.
43. Shibatani T, et al. (2006) Global organization and function of mammalian cytosolic proteasome pools: Implications for PA28 and 19S regulatory complexes. *Mol Biol Cell* 17:4962–4971.
44. Huttlin EL, et al. (2015) The BioPlex network: A systematic exploration of the human interactome. *Cell* 162:425–440.
45. Rouillard AD, et al. (2016) The harmonizome: A collection of processed datasets gathered to serve and mine knowledge about genes and proteins. *Database (Oxford)* 2016:baw100.
46. Li J, Rechsteiner M (2001) Molecular dissection of the 11S REG (PA28) proteasome activators. *Biochimie* 83:373–383.
47. Craig R, Cortens JP, Beavis RC (2004) Open source system for analyzing, validating, and storing protein identification data. *J Proteome Res* 3:1234–1242.
48. Salvi M, Sarno S, Cesaro L, Nakamura H, Pinna LA (2009) Extraordinary pleiotropy of protein kinase CK2 revealed by weblogo phosphoproteome analysis. *Biochim Biophys Acta* 1793:847–859.
49. Gao Y, Wang HY (2006) Casein kinase 2 is activated and essential for Wnt/beta-catenin signaling. *J Biol Chem* 281:18394–18400.
50. Sugiyama M, et al. (2013) Spatial arrangement and functional role of α subunits of proteasome activator PA28 in hetero-oligomeric form. *Biochem Biophys Res Commun* 432:141–145.
51. Raule M, et al. (2014) PA28αβ reduces size and increases hydrophilicity of 20S immunoproteasome peptide products. *Chem Biol* 21:470–480.
52. Tapia O, et al. (2012) Reorganization of Cajal bodies and nucleolar targeting of coilin in motor neurons of type I spinal muscular atrophy. *Histochem Cell Biol* 137:657–667.
53. Lefebvre S, et al. (1995) Identification and characterization of a spinal muscular atrophy-determining gene. *Cell* 80:155–165.
54. Lemm I, et al. (2006) Ongoing U snRNP biogenesis is required for the integrity of Cajal bodies. *Mol Biol Cell* 17:3221–3231.
55. Liu Q, Dreyfuss G (1996) A novel nuclear structure containing the survival of motor neurons protein. *EMBO J* 15:3555–3565.
56. Carmo-Fonseca M, Ferreira J, Lamond AI (1993) Assembly of snRNP-containing coiled bodies is regulated in interphase and mitosis–Evidence that the coiled body is a kinetic nuclear structure. *J Cell Biol* 120:841–852.